WATER RESOURCES RESEARCH, VOL. 27, NO. 10, PAGES 2759–2769, OCTOBER 1991

A Transfer Function Approach to Sampling Network Design for Groundwater Contamination

ROKO ANDRICEVIC AND EFI FOUFOULA-GEORGIOU

St. Anthony Falls Hydraulic Laboratory, Civil and Mineral Engineering Department, University of Minnesota, Minneapolis

This study presents a new methodology for designing and analyzing three-dimensional sampling networks for groundwater quality monitoring. Sampling design is represented in the frequency domain as a transfer function acting on the concentration spectrum to provide the sampling error variance, which is used as a measure of sampling performance. The presented methodology does not require numerical solution of either flow or transport equations; it operates directly on the statistics of the concentration field evaluated using a spectral representation. It also separates sampling design issues from the statistics of the aquifer properties, allowing better understanding of the influence of the subsurface characteristics on sampling error and therefore on sampling network design. The results show that sampling of groundwater quality should be viewed as a three-dimensional activity with two major design parameters: spatial spacing between wells (Δl_i, $i = 1, 2, 3$) and total number of wells. In the horizontal plane there is a clear need for anisotropy in spacing between wells with larger spacing needed in the direction of the mean flow than in the perpendicular direction. The sampling anisotropy ratio $\Delta l_1/\Delta l_2$ is found to be a function of the correlation structure of the hydraulic conductivity field and number of wells. The presented example demonstrates how sampling network design guidelines can be developed as functions of the statistical structure of the hydraulic conductivity field and other transport parameters.

1. INTRODUCTION

The extensive use of groundwater resources has increased the need for developing methodologies for sampling network design in order to provide an indication of the degree to which the subsurface environment has been affected by human activities. Subsurface groundwater quality monitoring is an expensive, time-consuming and uncertain process of characterizing the solute concentration which exhibits high variability in the subsurface environment.

A number of methodologies have been proposed over the years for groundwater sampling network design. These include mixed-integer programming [*Hsu and Yeh*, 1989], kriging and cokriging application [*Carrera et al.*, 1984; *McLaughlin and Graham*, 1986], variance reduction analysis [*Rouhani*, 1985], nearest neighbor approach [*Olea*, 1984], and methods based on optimization [e.g., *Hsueh and Rajagopal*, 1988; *Loaiciga*, 1989; *Andricevic*, 1990*a*; *ASCE Task Committee on Geostatistical Techniques in Geohydrology*, 1990*a*, *b*] and simulation [e.g., *Meyer and Brill*, 1988; *Massmann and Freeze*, 1987; *Van Geer*, 1987]. Some of these methods focus on discriminating among a finite set of alternatives and on sequentially adding new sampling locations based on error variance reduction. In classical optimization-simulation approaches numerical modeling of flow and transport cannot be avoided and therefore sampling network design depends upon the grid configuration used to perform the numerical flow and concentration simulations. As pointed out by *Moss* [1979] modeling error can be seen as a third dimension in network design and serves as a control (limitation) on the space-time trade-off that may be available to the network designer [*Andricevic*, 1990*a*]. In the geostatistical methodology (e.g., kriging) sampling network design [*Carrera et al.*, 1984] is based on estimating the point or spatial averaged concentration variances. This requires a substantial amount of existing data to estimate the sample variogram, particularly to estimate the variogram range. Since the data are usually limited for newly discovered concentration plumes, the sample estimation of variograms is impractical. An alternative is to use covariances to describe the spatial statistical dependence. The covariances are usually estimated either through first-order analysis of the numerical solution of flow and transport equations [*Loaiciga*, 1989; *Andricevic*, 1990*a*] or by applying inverse Fourier transform on spectra of concentration, head and hydraulic conductivity [*McLaughlin and Graham*, 1986]. In both cases heavy computations are needed to arrive at covariances, and finally the kriging weights associated with the potential sampling points need to be evaluated by solving a constrained minimization of the kriging equations. Since this has to be repeated every time a new sampling location is selected, only a finite set of monitoring alternatives is usually tested [*Carrera et al.*, 1984; *Loaiciga*, 1989; *Andricevic*, 1990*a*].

The purpose of this paper is to introduce a new sampling design methodology which requires neither numerical modeling of flow and transport nor estimation of covariances and which separates the space-time network design from the statistics of the aquifer properties, allowing better understanding of the influence of subsurface characteristics (e.g., hydraulic conductivity field) on the sampling error and therefore on the selected network design. The presented study will attempt to answer the following questions: What is the necessary spatial (three-dimensional) spacing in order to satisfy a desired sampling performance within the monitoring domain? How can the correlation structure of the hydraulic conductivity field be used in guiding the selection of sampling network design for groundwater contamination? The proposed methodology follows a transfer function approach and develops a framework suitable for analysis and design of three-dimensional sampling networks for groundwater quality. In contrast to other approaches, by working in

Paper number 91WR01391.
0043-1397/91/91WR-01391$05.00

the frequency domain, sampling is represented as a discrete spatial linear filter acting on the concentration field to give an estimate of the average concentration over the monitoring domain (whose size and location can be arbitrary) and averaging is represented by a continuous filter acting on the concentration field. The difference of these two filters (continuous minus discrete) is the transfer function used in computing the sampling error in estimating the average concentration over the monitoring domain. When the square of this transfer function is multiplied by the concentration spectrum and integrated over the frequency domain, the sampling error variance is obtained. The fact that the transfer function is separated from the statistics of the measured field (concentration spectrum) and that estimation of the covariance of the concentration field is avoided allows the network designer to choose a sampling pattern (based on a desired monitoring performance level prespecified in terms of a tolerable error variance) which is an explicit function of the hydraulic conductivity field statistics. An inherent disadvantage of the proposed transfer function sampling methodology is the sensitivity of the error variance on the mean concentration gradient which is constrained by the assumptions of the spectral approach. More discussion about this issue is left for the application study.

The idea of local averaging has been extensively used in modeling random fields [e.g., *Vanmarcke*, 1983] and especially in modeling hydrologic processes such as rainfall [e.g., *Rodriguez-Iturbe*, 1986]. Sampling network design based on the "sampling theorem" was employed by *Bras and Rodriguez-Iturbe* [1985, p. 175] while a transfer function approach was employed by *North and Nakamoto* [1989] for the purpose of comparing different rainfall measuring devices such as satellites and rain gages in terms of accurately estimating rainfall averages over a space-time domain. The weak point in their study was the lack of realistic spectra for rainfall fields since the complexity of that process [e.g., *Kumar and Foufoula-Georgiou*, 1989] does not permit a simple representation of the process in terms of the governing physical equations. On the other hand, spectral representations of subsurface processes are available [e.g., *Gelhar and Axness*, 1983] and therefore for these processes the advantages of a transfer function approach to sampling network design can be fully realized. The sampling network is represented in this work with two design parameters: spatial spacing between sampling points and total number of wells. The proposed methodology explicitly quantifies the influence of the hydraulic conductivity variance and correlation structure on the design parameters. It is also found that in the horizontal plane the spacing between wells must exhibit anisotropy with larger spacing needed in the direction of the mean flow than in the perpendicular direction. Although this is intuitively expected due to the anisotropy in the concentration field correlation structure, our methodology provides a formal procedure of quantifying sampling anisotropy and developing fairly general criteria for sampling network design based on the statistics of the hydraulic conductivity field. The presented methodology can also accommodate a sequential or staged monitoring program which permits one to update the network design when new information becomes available. The three-dimensional sampling network design methodology is fully demonstrated for the case of a continuous input nonreactive solute.

2. Transfer Function Approach to Sampling

Consider a random field $\psi(\mathbf{r})$, $\mathbf{r}\varepsilon\mathcal{R}^d$ defined in a d-dimensional space. Let the ensemble average of $\psi(\mathbf{r})$ be zero and its variance at a point in $\mathcal{R}^d$ be σ^2. We assume that the field $\psi(\mathbf{r})$ is weakly statistically homogeneous in space, i.e., the first two moments do not change with translation. In what follows we will present for simplicity the development of the transfer function methodology to sampling network design for the case of a one-dimensional field for which the vector $\mathbf{r}$ is replaced by the scalar l. Extension to multidimensional processes is straightforward and will be outlined in the next section.

Let $\Psi_L(x)$ denote the averaged process over an interval L (size of monitoring domain) centered at location x, i.e.,

$$\Psi_L(x) = \frac{1}{L}\int_{x-L/2}^{x+L/2} \psi(l)\, dl \tag{1}$$

and $\hat{\Psi}_L(x)$ denote its estimator obtained by averaging N sampled values of $\psi(l)$ taken in intervals Δl ($N\Delta l = L$)

$$\hat{\Psi}_L(x) = \frac{1}{N}\sum_{n=0}^{N-1} \psi[n\Delta l]$$

$$= \frac{1}{N}\int_{x-L/2}^{x+L/2}\sum_{n=0}^{N-1} \psi(l)\delta[l - n\Delta l]\, dl \tag{2}$$

where $\delta(\ )$ is the Dirac delta function. Both $\Psi_L(x)$ and $\hat{\Psi}_L(x)$ can be seen as random variables resulting from the random field $\psi(l)$ passing through the two linear filters $p(l)$ and $\hat{p}(l)$, respectively, as defined below:

$$\begin{aligned} p(l) &= 1/L \qquad x - L/2 \le l \le x + L/2 \\ p(l) &= 0 \qquad \text{otherwise} \end{aligned} \tag{3}$$

$$\begin{aligned} \hat{p}(l) &= \frac{\Delta l}{L}\sum_{n=0}^{N-1} \delta[l - n\Delta l] \qquad x - L/2 \le l \le x + L/2 \\ \hat{p}(l) &= 0 \qquad \text{otherwise} \end{aligned} \tag{4}$$

that is, $p(l)$ represents an averaging window of length L centered at location x while $\hat{p}(l)$ is its counterpart in the discrete domain. Let $\varepsilon_L(x) = \Psi_L(x) - \hat{\Psi}_L(x)$ denote the error in estimating the averaged process $\Psi_L(x)$. Note that since the ensemble average of $\psi(l)$ is zero $\hat{\Psi}_L(x)$ is an unbiased estimate of $\Psi_L(x)$ and thus $E[\varepsilon_L(x)] = 0$. The variance of the error (abbreviated here as ε)

$$\sigma_\varepsilon^2 = E[\varepsilon^2] = E[(\Psi_L(x) - \hat{\Psi}_L(x))^2] \tag{5}$$

can be seen as a measure of the accuracy in estimating the averaged process $\Psi_L(x)$ and therefore as a measure of sampling performance. Note that depending on the selection of the location x and size L of the averaging window, $\Psi_L(x)$ can be seen as the spatially averaged concentration over the entire monitoring domain (large L) or it can be seen as the spatially averaged concentration evaluated over a moving averaging window (small L compared to the size of entire monitoring domain) located at any point x within the domain

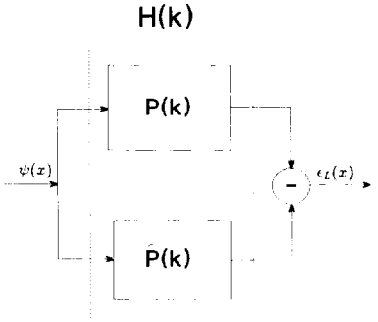

Fig. 1. Schematic representation of the transfer function approach to sampling (see text for definition of terms).

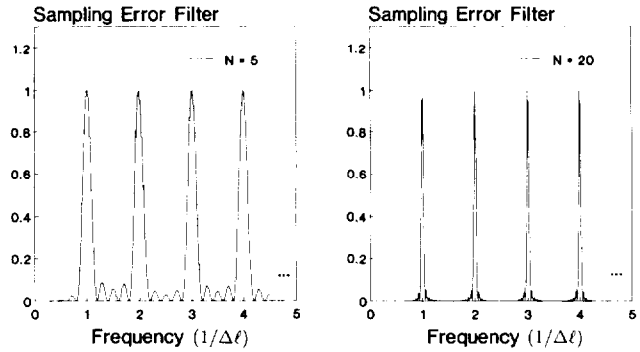

Fig. 2. Sampling error filter $|H(k)|^2$ as a function of frequency $(1/\Delta l)$ for (*a*) number of samples $N = 5$, and (*b*) $N = 20$.

of interest. The second interpretation might be more interesting in some cases since by moving the averaging window over the entire region one obtains a smoothed version of the contaminant plume.

Following results in spectral theory [*Blackman and Tukey*, 1959] the mean square error can be written in the frequency domain as

$$\sigma_\epsilon^2 = \int_{-\infty}^{+\infty} |H(k)|^2 S_\psi(k)\, dk \tag{6}$$

where $S_\psi(k)$ is the spectral density function of the random field $\psi(l)$ and k is the angular wave number (radians per unit length). The term $H(k)$ denotes the frequency response or transfer function of the system (see Figure 1) and is given as

$$H(k) = P(k) - \hat{P}(k) \tag{7}$$

where $P(k)$ and $\hat{P}(k)$ are the Fourier transforms of the uniform smoothing filter $p(l)$ and the discrete sampling filter $\hat{p}(l)$, respectively. $P(k)$ is given as

$$P(k) = \frac{\sin(kL/2)}{kL/2} \equiv B(kL/2) \tag{8}$$

which is known as the Bartlett filter or window of length L [*Blackman and Tukey*, 1959] and will be denoted herein as $B(\pi kL)$. $\hat{P}(k)$ takes the form (see the appendix)

$$\hat{P}(k) = \frac{\sin(kN\Delta l/2)}{N \sin(k\Delta l/2)} \tag{9}$$

The square of the transfer function $|H(k)|^2$ can be seen as the sampling error filter in the frequency domain which is design-dependent and acts on the spectrum of the original random field we wish to monitor. Using the above expressions for $P(k)$ and $\hat{P}(k)$ and after some rearrangements, it can be further shown that $|H(k)|^2$ can be written as

$$|H(k)|^2 = \frac{1}{N^2} \frac{\sin^2(kN\Delta l/2)}{\sin^2(k\Delta l/2)} \left[1 - \frac{\sin(k\Delta l/2)}{k\Delta l/2}\right]^2 \tag{10}$$

(see also *North and Nakamoto* [1989]). It is important to note from (6) that the sampling error filter (which explicitly relates to sampling network design via its dependence on sample spacing Δl and total number of wells N) is separated from the statistics of the concentration field (summarized in its spectrum). For example, by changing the parameters of the sampling error filter (number of samples, spacing) one can directly study the influence on the sampling error variance regardless of the concentration spectrum. This allows a network designer to systematically analyze what aspects of the concentration field (transport parameters, hydraulic conductivity field characteristics) contribute most to sampling performance. Note that in other approaches, e.g., kriging, this separability property is not present since the spectrum or covariance is evaluated based upon the measurement locations.

To get an insight of the proposed sampling methodology it is helpful to study the form of the sampling error filter $|H(k)|^2$. This is plotted in Figure 2 for two values of N ($N = 5$ and $N = 20$). It is seen that the sampling error filter in the frequency domain represents a series of spikes at frequencies $f = kn/2\pi = n/\Delta l$, for all integers n except zero where it vanishes due to the second factor on the right-hand side of (10) which is zero at the origin. The sampling performance is therefore described by multiplying this filter with the spectrum of the concentration field. In other words, the sampling error filter, as plotted in Figure 3*a*, is multiplied by the concentration spectrum (plotted on the same figure) to produce the sampling error spectrum (solid line) and the area under this spectrum gives the sampling error variance σ_ϵ^2. The magnitude of the error variance clearly depends on the starting frequency of the error filter and all harmonics of it. It is important to notice that the starting frequency of the error filter is $1/\Delta l$. This means that having small Δl makes the starting frequency larger and consequently the error vari-

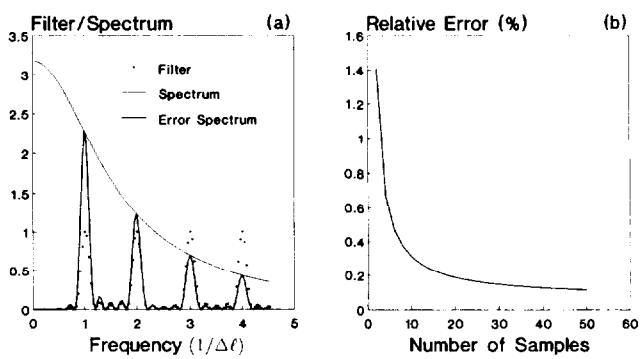

Fig. 3. (*a*) The sampling error spectrum as a result of multiplying the sampling error filter with the spectrum of the measured process. (*b*) Comparison of the variance of sampling error (σ_ϵ^2) computed using the exact integration and the Dirac comb approximation for different numbers of samples.

ance smaller. At the limit (of theoretical but no practical interest) Δl can be chosen as corresponding to a starting frequency at which the spectrum of the concentration field approaches zero (sampling theorem). In that case, σ_ε^2 will approach zero (neglecting the measurement error) but Δl will be impractically small.

An important aspect of the sampling error filter is the sensitivity of its shape on the number of samples. It is clear that by increasing the number of samples the spikes are getting narrower and lobes between spikes are disappearing (see Figure 2). Asymptotically this can be written as

$$\lim_{N\to\infty}\left\{\frac{1}{N^2}\frac{\sin^2(kN\Delta l/2)}{\sin^2(k\Delta l/2)}\left[1-\frac{\sin(k\Delta l/2)}{k\Delta l/2}\right]^2\right\}$$

$$=\frac{1}{N\Delta l}\sum_{n=-\infty,n\neq 0}^{\infty}\delta\left(k-\frac{2\pi n}{\Delta l}\right) \qquad (11)$$

which is a series of spikes at $f = n/\Delta l$ for all positive and negative integers n and is known as the Dirac comb [*Blackman and Tukey*, 1959]. Note that the summation index ($n = -\infty$ to $+\infty$) of (11) refers to the number of spikes (harmonics) of the Dirac comb (see Figure 2) and does not relate to the number of wells N. Under the assumption of large N the filter can be approximated as

$$|H(k)|^2 \cong \frac{1}{N\Delta l}\sum_{n=-\infty,n\neq 0}^{\infty}\delta\left(k-\frac{2\pi n}{\Delta l}\right) \qquad (12)$$

By substituting in (6) and using the shifting property of the delta function, an approximate expression for the sampling error variance can be obtained as

$$\sigma_\varepsilon^2 \cong \frac{2}{L}\sum_{n=1}^{\infty} S_\psi\left(\frac{2\pi n}{\Delta l}\right) \qquad (13)$$

Note that the filter $|H(k)|^2$, which acts on the spectrum $S_\psi(k)$, picks up contributions to the sampling error from the spectrum at twice the Nyquist frequency ($1/2\Delta l$) and all the harmonics of it. The convergence of the summation in (13) is fast due to the fast decay of the spectrum of the random field at high frequencies. It is worth studying the accuracy in estimating the sampling error variance σ_ε^2 by the approximate expression (13) since this provides significant computational advantages. This accuracy is studied below for a simple one-dimensional example.

Figure 3*a* shows the sampling error filter for $N = 5$ acting on the hypothetical spectrum

$$S_\psi(k) = \frac{\sigma^2}{\pi(1+k^2\lambda^2)} \qquad (14)$$

evaluated for parameters $\sigma^2 = 10$ and $\lambda = 0.1$. The bold line denotes the integrand of (6) which represents the sampling error spectrum and the area under this function represents the sampling error variance. The integrand has spikes at frequency $1/\Delta l$ and all the harmonics of it and each spike has a bandwidth equal to $2/N\Delta l$. Thus by examining the approximation by Dirac comb in (12) it can be seen that the approximation replaces the spikes with rectangles of area $1 \times N\Delta l$ and neglects the lobes between the spikes. By increasing the number of samples the approximation becomes better since the lobes between spikes disappear and the spikes become narrower and are better approximated with narrow rectangles. In Figure 3*b* the relative error between the approximation and numerical integration of (6) is presented as a function of the number of samples. The relative error is defined as

$$\xi = \frac{\sigma_a^2 - \sigma_i^2}{\sigma_a^2}\,100 \qquad (15)$$

where σ_a^2 and σ_i^2 denote the approximated and integrated sampling error variance, respectively. It is clear that the relative error is rapidly reduced by increasing the number of samples and for the one-dimensional sampling case the Dirac comb approximation has a relative error of less than 0.5% for $N = 6$. Note also that the Dirac comb approximation gives a conservative estimate of the sampling error variance ($\sigma_a^2 > \sigma_i^2$). Therefore for all practical purposes the approximation in (12) represents an accurate estimation of the sampling error variance as defined in (6). In fact, by considering the sampling design in three dimensions three filters would be multiplied together, thus rapidly reducing the magnitude of the lobes between the spikes, and in that case the approximation is even closer to the exact integration.

Before we proceed with the development of the sampling error variance of the concentration field, it should be emphasized that in the development of (6) the measurement error was neglected for simplicity. This, however, can be easily accounted for, in which case the expression for the sampling error variance becomes

$$\sigma_\varepsilon^2 = \int_{-\infty}^{+\infty}|H(k)|^2 S_\psi(k)\,dk + \int_{-\infty}^{+\infty}|\hat{P}(k)|^2 S_N(k)\,dk \qquad (16)$$

where $\hat{P}(k)$ is given by (9) and $S_N(k)$ is the spectrum of the measurement noise.

3. Sampling Error Variance of a Steady State Three-Dimensional Concentration Field

Of particular practical interest is the ability to design a three-dimensional sampling network for the purpose of monitoring a concentration plume. As we have seen from the previous section, evaluation of the sampling error variance requires evaluation of the structure of the concentration spectrum in three dimensions.

The general equation describing the transport of an ideal nonreactive, conservative solute in a saturated porous medium is given by

$$\theta\frac{\partial c}{\partial t} + q_i\frac{\partial c}{\partial x_i} = \frac{\partial}{\partial x_i}\left(E_{ij}\frac{\partial c}{\partial x_j}\right) \qquad (17)$$

where summation is implied for repeated indices, θ is porosity, q_i is specific discharge in the x_i direction, and $E_{i,j}$ is the local bulk dispersion coefficient tensor. Following the small perturbation approach, the log hydraulic conductivity, specific discharge, and concentration are decomposed into a mean and a small perturbation about the mean

$$\ln K = f = F + f'$$

$$q_i = \bar{q}_i + q_i' \qquad i = 1, 2, 3 \tag{18}$$

$$c = \bar{c} + c'$$

where the perturbation quantities f', q', and c' have zero mean and they are assumed to be locally stationary (statistically homogeneous). The assumption about local statistical homogeneity for the concentration fluctuations is based on the assumption that the mean concentration gradient varies slowly relative to the scale of concentration fluctuations. The range of validity of uniformity of the mean concentration gradient depends on the case at hand. The mean concentration gradient is usually estimated in practice either using physically based deterministic models (e.g., Gaussian plume model using effective and uniform parameters) or using available field data and statistical analysis.

By representing the perturbed quantities through Fourier-Stieltjes integrals and applying them on the mean removed transport equation the spectrum of the steady concentration field is obtained [*Vomvoris and Gelhar*, 1990]

$$S_{cc}(\mathbf{k}) = \frac{1}{q^2} \frac{J_{c_i} J_{c_j}}{k_1^2 + [\alpha_L k_1^2 + \alpha_T (k_2^2 + k_3^2)]^2} S_{q_j q_i}(\mathbf{k}) \tag{19}$$

where $q = q_1$ is the mean specific discharge obtained by aligning the x_1 direction to the direction of the mean flow, $S_{q_j q_i}(\mathbf{k})$ is the three-dimensional spectrum of the specific discharge along the x_j and x_i axes ($j, i = 1, 2, 3$), $J_{c_j} = -\partial \bar{c}/\partial x_j$ is the mean concentration gradient assumed locally (within the monitoring domain) constant, and $\mathbf{k} = (k_1, k_2, k_3)$ is the three-dimensional wave number vector. The spectrum of the specific discharge $S_{q_j q_i}(\mathbf{k})$ is related to the spectrum of the log hydraulic conductivity $S_{ff}(\mathbf{k})$ as follows:

$$S_{q_j q_i}(\mathbf{k}) = K_g^2 J_m J_n \left(\delta_{jm} - \frac{k_j k_m}{k^2}\right)\left(\delta_{in} - \frac{k_i k_n}{k^2}\right) S_{ff}(\mathbf{k}) \tag{20}$$

where k is the wave number magnitude, δ_{jm} denotes the Kronecker delta, $K_g = \exp[E(\ln K)] = \exp(F)$ is the geometric mean of the hydraulic conductivity and summation over m and n is implied. More details and discussion about the spectrum of the concentration field and specific discharge can be found in the work by *Gelhar and Axness* [1983].

The sampling error filter (10) is extended to three dimensions by considering the monitoring domain as a sampling volume box $L_1 \times L_2 \times L_3$, where, e.g., L_1 is the length of monitoring in the x principal direction given as the product of number of wells and spacing between wells. Using (8) and with some algebraic manipulations it can be shown that the sampling error filter in three dimensions has the following form:

$$|H(k)|^2 = B^2(k_1 L_1/2) B^2(k_2 L_2/2) B^2(k_3 L_3/2) \cdot \left[1 - \frac{1}{B(k_1 \Delta l_1/2) B(k_2 \Delta l_2/2) B(k_3 \Delta l_3/2)}\right]^2 \tag{21}$$

where $B^2(k_1 L_1/2)$ and $B^2(k_1 \Delta l_1/2)$ denote the square of the Bartlett filter of length L_1 and Δl_1, respectively.

The sampling error variance of σ_ϵ^2 can then be evaluated from (6) or using the Dirac comb approximation as

$$\sigma_\epsilon^2 \cong \frac{8}{L_1 L_2 L_3} \sum_{n_1=1, n_2=1, n_3=1}^{\infty} S_{cc}\left(\frac{2\pi n_1}{\Delta l_1}, \frac{2\pi n_2}{\Delta l_2}, \frac{2\pi n_3}{\Delta l_3}\right) \tag{22}$$

The summation in (22) does not include integers $n_i = 0$ since the sampling error filter in (21) vanishes for zero wave numbers. This fact turns out to be important in determining the shape of the ln K conductivity spectrum and will be discussed more in the three-dimensional example presented in the following section.

The first frequency around which our sampling error filter picks up the variability of the concentration spectrum is at $f_i = 1/\Delta l_i$, where i denotes the ith principal direction. In the case of sampling the concentration field, the frequency $1/\Delta l_i$ represents the highest contribution from the concentration power spectrum to the sampling error variance (see Figure 3*a*). In fact, this starting frequency and the corresponding energy (variability) of the concentration spectrum will serve as a guideline for the selection of proper spacing between wells such that a certain monitoring performance level is achieved.

4. Three-Dimensional Sampling Design of a Continuous Concentration Input

In order to demonstrate the proposed methodology of sampling design and analysis we consider a hypothetical case of an underground tank leaking a conservative nonreactive solute at a constant rate m in a three-dimensional aquifer with steady groundwater flow velocity. By selecting the coordinates such that the origin is at the injection point ($x = y = z = 0$), the resulting steady mean concentration distribution for $x \gg y, z$ can be approximated as [*Vomvoris and Gelhar*, 1990]

$$\bar{c}(x, y, z) \cong \frac{m}{4\pi\theta (A_{22} A_{33})^{1/2} x v} \exp\left[-\left(\frac{y^2}{4A_{22}x} + \frac{z^2}{4A_{33}x}\right)\right] \tag{23}$$

where A_{22} and A_{33} are the lateral macrodispersivities along the y and z principal directions, respectively; θ is the porosity; m is the rate of the injected mass; and v is the mean flow velocity assumed along the x axis. For this example we have used the following set of parameters: $A_{22} = A_{33} = 0.01$ m, $\theta = 0.3$, $m = 1$ (unit mass), and $v = 0.05$ m/day. The mean concentration gradient in the three principal directions is obtained by differentiating (23):

$$\partial \bar{c}/\partial x = \bar{c} \frac{1}{x}\left[-1 + \left(\frac{y^2}{4A_{22}} + \frac{z^2}{4A_{33}x}\right)\frac{1}{x}\right] \tag{24}$$

$$\partial \bar{c}/\partial y = \bar{c}\left[\frac{-y}{2A_{22}x}\right] \tag{25}$$

$$\partial \bar{c}/\partial z = \bar{c}\left[\frac{-z}{2A_{33}x}\right] \tag{26}$$

Using (23)–(26) the concentration spectrum in (19) can be evaluated with the choice of the ln K conductivity spectrum $S_{ff}(\mathbf{k})$. *Vomvoris and Gelhar* [1990] in their study of evalu-

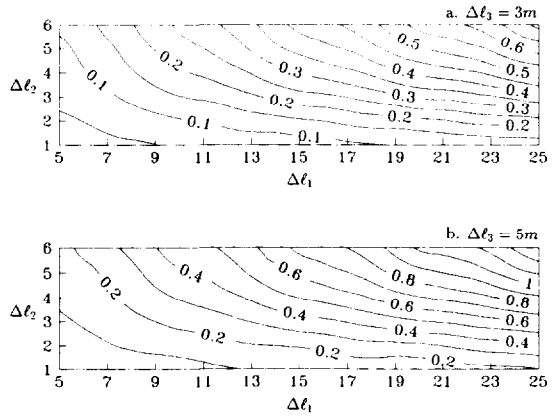

Fig. 4. Sampling error index I_ε as a function of spacing between wells in the direction of flow (Δl_1) and perpendicular direction (Δl_2). The sampling spacing in the vertical direction is fixed to (*a*) $\Delta l_3 = 3$ m and (*b*) $\Delta l_3 = 5$ m. The monitoring domain is $100 \times 60 \times 30$ m; isotropic ln K field with $\lambda_1 = \lambda_2 = \lambda_3 = 2$ m and $\sigma_f^2 = 1$.

ating the concentration variance (using the same example), suggested a "hole type" spectrum for the ln K field. The main characteristic of such a ln K spectrum is the zero integral scale which implies that there is minimal variance contribution for small wave numbers (spectrum is zero at origin) and that the correlation becomes negative after a certain separation distance. This restriction on the shape of the ln K spectrum is a clear mathematical necessity (there is no strong field evidence of such behavior for the hydraulic conductivity) in order to have finite concentration variance which can be obtained by integrating the spectrum in (19). Note, however, that this assumption can be relaxed when the proposed transfer function approach is used for sampling network design. This is because the sampling error filter of (10) acts on the concentration spectrum at frequencies $n/\Delta l_i$ except at zero where it vanishes (see, for example, Figure 2). In fact, the discrete filter will sample at the origin only asymptotically when $\Delta l_i \to \infty$ (i.e., no measurements within the domain). Therefore in the evaluation of the sampling error variance, there is no need to enforce the zero integral scale of the input ln K correlation structure.

In this study we assume that the ln K field has a negative exponential correlation structure and therefore its spectrum has the following form [*Gelhar and Axness*, 1983]:

$$S_{ff}(\mathbf{k}) = \frac{\sigma_f^2 \lambda_1 \lambda_2 \lambda_3}{\pi^2[1 + (k_1\lambda_1)^2 + (k_2\lambda_2)^2 + (k_3\lambda_3)^2]^2} \qquad (27)$$

where σ_f^2 is the variance of the ln K field and λ_i is the correlation scale in the ith principal direction.

The sampling performance, measured by the sampling error variance σ_ε^2, is normalized with respect to the mean concentration ($\bar{c}$) over the sampling domain to yield a sampling error index

$$I_\varepsilon = (\sigma_\varepsilon/\bar{c})100 \qquad (28)$$

The sampling error index will be used throughout the paper to represent the sampling network performance.

Figures 4*a* and 4*b* show the sampling error index I_ε plotted as a function of the spacing between wells in the direction of mean flow (Δl_1) and perpendicular to the mean flow (Δl_2), for a fixed spacing in the vertical direction $\Delta l_3 = 3$ m and 5 m, respectively. The input ln K field is isotropic with variance equal to one and correlation scale equal to 3 m. In the direction of the mean flow Δl_1 ranges from 4 m to 24 m and in the perpendicular direction Δl_2 is varied between 1 m and 6 m. In Figures 4*a* and 4*b* the lines of equal sampling error index represent the trade-off between monitoring well spacing in the two directions of the horizontal plane for fixed spacing in the vertical direction. In other words, a different combination of spacing in the x and y directions can achieve the same sampling performance. As expected, the sampling performance clearly shows (by the slope of the lines of equal sampling error index) the need to have much closer spacing in the direction perpendicular to the mean flow than in the direction of flow. This important sample spacing ratio, $\Delta l_1/\Delta l_2$, will be called herein anisotropy in horizontal spacing (AHS). The smaller spacing in the direction perpendicular to the mean flow was expected since the concentration field exhibits a high degree of anisotropy with a much higher correlation scale in the direction of the mean flow than in the perpendicular direction. This was also observed by *Vomvoris and Gelhar* [1990] by analyzing the concentration covariance and was also shown in numerical simulations by *Graham and McLaughlin* [1989*a*]. By infrequent sampling in the vertical direction (larger Δl_3) the overall sampling error is increased (higher error index) by approximately 40% (Figure 4*b*) illustrating the importance of considering the sampling network design of groundwater quality as a three-dimensional monitoring activity. In reality the vertical sampling is usually performed with multicompletion wells (a cluster of wells with each one screened at different depth) and the proposed approach provides a way of choosing an appropriate spacing in the vertical direction in order to capture the concentration plume variability. In this way a network designer can trade off the extensive cost of such a cluster of wells with needed accuracy of estimating the vertical extent of the contaminant plume.

In Figures 5*a* and 5*b* sampling performance in the vertical plane is depicted. Spacing in the direction perpendicular to the mean flow was fixed at $\Delta l_2 = 2$ and 4 m. The analysis shows that the sampling error index is increased 5 times by going from $\Delta l_2 = 2$ m to $\Delta l_2 = 4$ m. This clearly indicates the sensitivity of sampling performance to the choice of well spacing in the direction perpendicular to the mean flow. This

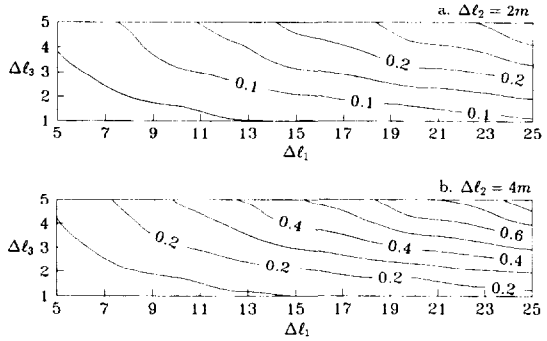

Fig. 5. Sampling error index I_ε as a function of spacing between wells in the direction of flow (Δl_1) and in the vertical direction (Δl_3). The sampling spacing in the direction perpendicular to the mean flow is fixed to (*a*) $\Delta l_2 = 2$ m and (*b*) $\Delta l_2 = 4$ m. The monitoring domain is $100 \times 60 \times 30$ m; isotropic ln K field with $\lambda_1 = \lambda_2 = \lambda_3 = 2$ m and $\sigma_f^2 = 1$.

sensitivity is a result of the small correlation scale in the direction perpendicular to the mean flow, suggesting therefore smaller spacing between sampling points in order to properly capture the concentration variability. It seems that the spacing between monitoring wells in the direction perpendicular to the mean flow is a crucial sampling network design parameter. Therefore, the AHS ratio can be seen as a major design feature for sampling network design of groundwater contamination. It obviously depends on the correlation scales of the concentration plume and should reflect the observed anisotropy in the concentration field. This is easily seen in the proposed transfer function approach since the persistence of variability for high wave numbers (tail of the spectrum), particularly in the direction perpendicular to the mean flow, indicates a strong need for closer spacing than in the direction of flow where the fast decay of the concentration spectrum allows a larger distance between the wells (see Figure 6). Note that this conclusion is based on the assumption of known direction of the mean flow and the selection of the stationary concentration spectrum in (19). The concentration spectrum in (19), developed by *Vomvoris and Gelhar* [1990], is highly dependent on the form of the ln K covariance function and results in a high longitudinal concentration correlation scale which indicates too large AHS ratios. However, if nonstationarity in the concentration spectrum is considered [*Li and McLaughlin*, 1991] the AHS ratio may be altered. This is one more reason to reexamine, in future research studies, a very common assumption about stationarity in the concentration field.

The correlation structure of the concentration field is spatially variable and results from the propagation of the underlying ln K correlation structure through the hydraulic head and velocity correlations. The fact that an isotropic ln K field does give rise to an anisotropic velocity field was demonstrated by *Bakr et al.* [1978] and *Graham and McLaughlin* [1989*a*]. In addition, the velocity correlation structure exhibits a hole effect correlation structure (negative correlation after some distance) in the transversal direction as was observed by *Rubin* [1990] and also shown through numerical simulations by *Morrison and Andricevic* [1991]. This fact can be seen from Figure 6 where the velocity spectrum in the horizontal plane (fixed vertical

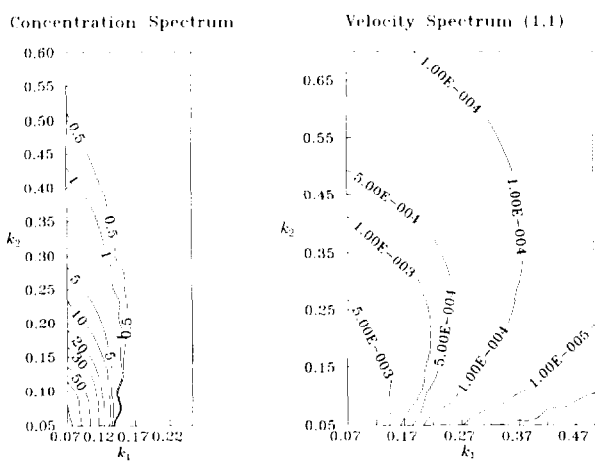

Fig. 6. (*a*) Concentration spectrum in the horizontal direction and (*b*) spectrum of the longitudinal velocity in the longitudinal direction. Here, k_1 and k_2 are wave numbers and k_3 is fixed to 0.01.

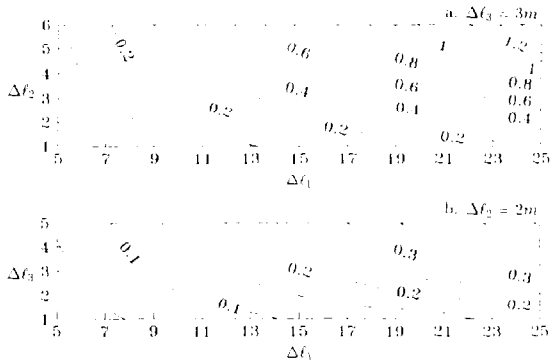

Fig. 7. As (*a*) Figure 4*a* and (*b*) Figure 5*a*, but for anisotropic ln K field with $\lambda_1 = 6$ m, $\lambda_2 = 2$ m and $\lambda_3 = 0.667$ m such that $\Lambda_a = (\lambda_1\lambda_2\lambda_3)^{1/3} = \lambda = 2$ m.

wave number k_3) exhibits a periodicity for several combinations of k_1 and k_2. Therefore, within the scope of sampling network design it is important to study how different characteristics of the ln K field affect sampling design and to demonstrate how this information can be used to provide guidance in practical situations.

4.1. *Effects of Anisotropic Conductivity Field*

Up to now we have analyzed an isotropic ln K field where the correlation scale is the same in every direction of the monitoring domain. In reality, this will seldom be the case and in most situations the ln K field will exhibit anisotropy. In Figures 7*a* and 7*b* the sampling performance is presented for the case of an anisotropic ln K field which has the geometric mean of its correlation scales equal to the correlation scale of the isotropic ln K field used to produce Figures 4*a* and 5*a*. This can be simply written as

$$\Lambda_a = (\lambda_1\lambda_2\lambda_3)^{1/3} = \lambda \tag{29}$$

where Λ_a is the geometric mean correlation scale of the anisotropic ln K field. In Figure 7*a* sampling performance is presented in the horizontal plane for fixed vertical sampling $\Delta l_3 = 3$ m; Figure 7*b* shows the vertical plane sampling design for fixed $\Delta l_2 = 2$ m. It is of particular interest to compare Figure 4*a* with Figure 7*a* and Figure 5*a* with Figure 7*b* since the only difference between them is the anisotropic ln K field used to produce Figures 7*a* and 7*b*. The important point to note is that the overall sampling performance is worse for anisotropic ln K fields, particularly for increased sample spacing in the x and y directions. This is possibly due to the increased variability in the direction perpendicular to the mean flow together with the reduced correlation scale in that direction.

This analysis shows that an anisotropic ln K field needs to be sampled differently from an isotropic field with correlation scale equal to the geometric mean of the anisotropic correlation scales if the same sampling performance is to be achieved . This is due to the different distribution of the variance (shape of spectrum) of the anisotropic ln K field although, as observed by *Vomvoris and Gelhar* [1990], the concentration variance between these two fields does not differ significantly.

Since the need for anisotropy in the horizontal spacing (AHS) between wells is intuitively obvious (and has been

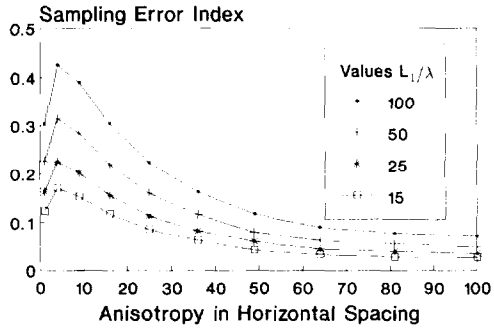

Fig. 8. Sampling error index I_ε as a function of the anisotropy in horizontal spacing (AHS = $\Delta l_1/\Delta l_2$) and for a fixed number of wells N = 240. Isotropic ln K field with λ varying from 1 to 7 m; fixed Δl_3 = 3 m and L_1 = 100 m. Figure shows different curves for different values of L_1/λ.

intuitively followed in some field applications [e.g., *Perlmutter and Lieber*, 1970]), it is of practical interest to formally analyze how the correlation structure of the ln K field affects the choice of AHS. In Figure 8 the sampling error index is plotted as a function of different anisotropy in horizontal sampling ratios (AHS = $\Delta l_1/\Delta l_2$) for a fixed total number of sampling wells within the monitoring domain, and for different magnitudes of the ratio of the length of the monitoring domain in the x direction relative to the correlation scale of the isotropic ln K field (L_1/λ). By increasing the AHS ratio the sampling performance is clearly improving up to $\Delta l_1/\Delta l_2 \cong 60$ after which further increase in AHS does not provide significant reduction in the sampling error. This observation has important implications for sampling network design since it indicates that in order to efficiently monitor the plume moving through an isotropic ln K field the distance between wells in the direction perpendicular to the mean flow must be smaller (approximately 60 times smaller for this example) compared to the well distance in the direction of flow regardless of the ln K correlation scale magnitude. Further increase in the anisotropy in spacing would only marginally improve the overall sampling activity and may not be a desirable monitoring option, keeping in mind that by placing wells further downstream one may miss the moving plume (or part of it) as happened for example in the initial sampling design of the Borden field tracer test (E. A. Sudicky, personal communication, 1990). This possible hit-or-miss characteristic is an important concern in practical monitoring schemes since the groundwater velocity field (which is the most important driving force) is highly uncertain in practical applications.

4.2. *Effect of Total Number of Wells*

In the previous example the total number of samples in the horizontal direction (monitoring wells) was kept constant in order to examine the relationship among the AHS, sampling error index, and correlation scales of the ln K field. However, the number of samples in the horizontal plane plays an important role in groundwater monitoring design due to the high cost of drilling an additional monitoring well. Clearly, an increase in the total number of samples within the monitoring domain would reduce the sampling error and as long as that increase in number of samples is followed by a significant reduction in sampling error the additional investment is justified. Figure 9*a* displays the sampling error index of an isotropic ln K field as a function of the total number of samples in the horizontal plane for different AHS. For smaller AHS a significant reduction in sampling error is achieved by increasing the total number of samples. However, once the AHS ratio becomes 50–60, further increase in the number of samples (above 200) hardly provides any further reduction in the sampling error. It is important to note that by increasing the AHS ratio a reduction in sampling error can be achieved with fewer wells within a fixed size monitoring domain. This may have a significant impact on the necessary monitoring budget. Note that this fact known as "decreasing marginal return" has been also found by *Andricevic* [1990*a*] in monitoring groundwater quantity. Observe that again an AHS ratio of 60 seems to be the point where further increase in AHS does not provide significant further decrease in the sampling error. In Figure 9*b* the same analysis is depicted for an anisotropic ln K field.

The above analysis clearly shows that AHS and total number of samples are related to each other and only a trade-off between them will lead to cost-effective sampling network design. If on top of that we add the characteristics of the ln K field the complete picture of the three-dimensional sampling network design for groundwater quality can be obtained.

Figure 10 represents the sampling error index for different combinations of AHS, number of samples and vertical anisotropy in the ln K field (Figure 10*a*, 160 wells; Figure 10*b*, 240 wells). This figure in conjunction with Figures 8 and 9 provides guidelines for determining the most appropriate AHS ratio for given ln K correlation scales, chosen number of samples (e.g., from Figure 8), and desirable degree of

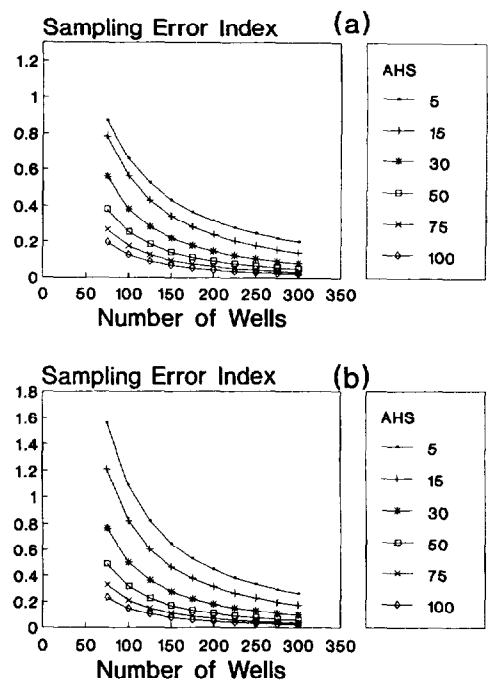

Fig. 9. Sampling error index I_ε as a function of horizontal number of samples (number of wells) and for different values of horizontal sampling anisotropy ratio AHS = $\Delta l_1/\Delta l_2$. The sampling spacing in the vertical direction is fixed to Δl_3 = 3 m. (*a*) Isotropic ln K field with λ = 3m. (*b*) Anisotropic ln K field with λ_1 = 9 m, λ_2 = 3 m and λ_3 = 1 m such that $(\lambda_1\lambda_2\lambda_3)^{1/3}$ = 3 m.

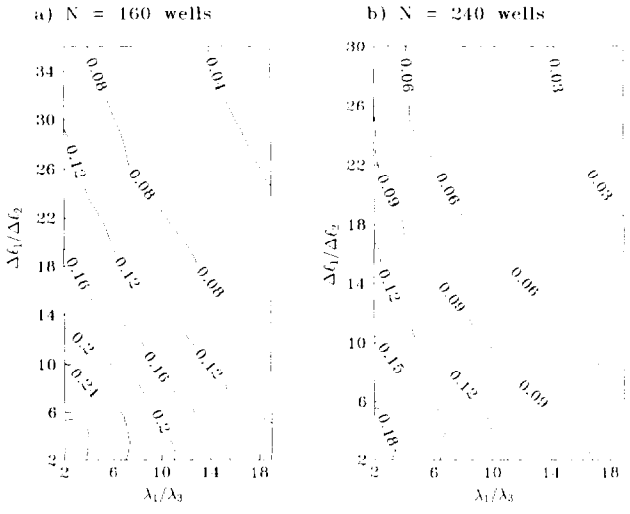

Fig. 10. Sampling error index I_ϵ as a function of anisotropy in horizontal spacing ration AHS = $\Delta l_1/\Delta l_2$ and vertical anisotropy in the ln K field correlation structure.

sampling error. For any given anisotropy in the ln K field, magnitude of correlation scales, and an acceptable sampling error the horizontal sampling anisotropy and number of wells can be found.

By examining Figure 10 closely it is clear that increased AHS does not provide the same improvement for different vertical anisotropy ratios in the ln K correlation scales. In fact, for significant anisotropy in the vertical direction (layered aquifer) only marginal improvement is achieved by increasing the AHS. In that case, only a further increase in the total number of samples per monitoring domain or an increased anisotropy in vertical spacing will result in better overall sampling performance. More uniformly structured aquifers (less anisotropy) will need to be sampled at a higher anisotropy ratio to produce a smaller sampling error.

In Figure 11 the sampling error index, I_ϵ, is depicted as a function of the ln K variance for different AHS ratios. It is important to notice that there is a certain AHS ratio (5–10) for which the sampling error is suddenly increased. This behavior is attributed to the shape of the concentration

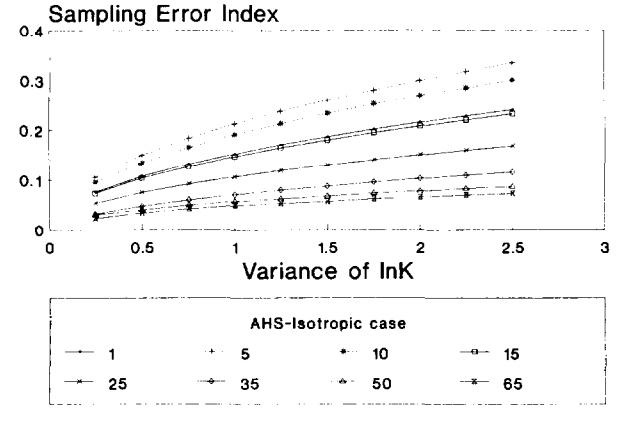

Fig. 11. Effect of the ln K field variance on the sampling error. Isotropic ln K with λ = 3 m. Fixed number of wells N = 240. Different curves are shown for different values of the anisotropy in horizontal spacing ratio AHS = $\Delta l_1/\Delta l_2$.

spectrum given by (19) (see Figure 6) from which it can be seen that for a small and fixed wave number k_3 (which corresponds to sparse sampling in the vertical direction) the concentration spectrum in the direction perpendicular to the mean flow has a flat region for a certain frequency span. Such a feature may indicate a periodicity in the direction perpendicular to the mean flow and results from the correlation structure of the concentration field which in the direction perpendicular to the mean flow has negative values at some distance ("hole effect") as has also been observed in the study by *Vomvoris and Gelhar* [1990]. If the frequency corresponding to the chosen spacing in the direction perpendicular to the mean flow (i.e., $1/\Delta l_2$) coincides with frequencies within that flat region we clearly have an increase in the sampling error.

5. Concluding Remarks

In this paper we presented a new methodology for designing and analyzing three-dimensional sampling networks for groundwater quality monitoring. Sampling network design is presented in the frequency domain as a transfer function acting on the concentration spectrum to provide the sampling error variance, which is used as a measure of sampling performance. The transfer function of the system depends on two important sampling design parameters: (1) spacing between samples Δl_i, i= 1, 2, 3 and (2) total number of samples N_i in each i direction. It is found that the sampling error is proportional to the concentration gradient and the variance of the ln K field while inversely proportional to the total number of samples within the monitoring domain and half the Nyquist frequency ($1/\Delta l_i$). This frequency determines the point where the concentration spectrum contributes to the sampling error the most. The smaller the spectral power at this frequency the better the performance of the monitoring network.

The proposed methodology for sampling network design allows the network designer to directly relate the sampling design parameters to statistical characteristics of the ln K field. It provides a convenient tool for practical implementation of sampling design as a three-dimensional monitoring activity, an attempt which to the best of our knowledge seems to be seldom reported in the literature.

The presented results show that sampling network design for groundwater quality should be devised as a three-dimensional sampling activity with particular emphasis on sampling in the direction perpendicular to the mean flow. In the horizontal plane, which is of high practical interest, there is a clear need for anisotropy in horizontal spacing between the wells with larger spacing needed in the direction of the mean flow and smaller spacing in the direction perpendicular to the flow. This intuitively expected feature is attributed to the higher correlation scale of the concentration plume in the mean flow direction. It is also found that the anisotropy in horizontal spacing ratio (AHS = $\Delta l_1/\Delta l_2$) is a function of the ln K field correlation scales and that an apparent trade-off exists between AHS and the total number of samples. In the case of significant vertical anisotropy in the ln K correlation field, the sampling design in the vertical direction also becomes an important network design parameter. Several guidelines are presented which can be used to analyze an existing monitoring network performance or to design a new one by choosing the proper spatial spacing of wells and the

total number of wells within the monitoring domain. Note that in evaluating the performance of an unevenly spaced existing monitoring network a representative "equivalent" spacing between wells in the two principal directions must be obtained. One way of doing this is to use Thiessen polygons to assign areas to every well and then compute an average well area which can be assigned to a rectangle of sides Δl_1 and Δl_2.

With the proposed methodology the sampling network design is clearly separated from the statistics of the concentration field, thus allowing a network designer to gain a better insight of how to go about sampling based on the known (or at least estimated) ln K field characteristics. This feature has a direct practical application to sampling design for field tracer test studies. Furthermore, the impact of the transport parameters on sampling design can be explicitly evaluated. Such an analysis may have a direct implication in inverse modeling where concentration data are used to estimate partially known hydrogeological parameters. Parameters significantly affecting sampling design are more likely to be identifiable through the inverse estimation process based on concentration measurements.

The correlation structure of the moving concentration plume is also temporally variable and (particularly in the case of nonconservative solutes) sequential sampling design might be desirable. The advantages of sequential sampling have been demonstrated by *Andricevic* [1990*b*] in monitoring and management of groundwater withdrawals and by *Graham and McLaughlin* [1989*b*] in predicting solute transport. For temporally variable concentration fields, the proposed methodology needs to be extended in the time domain (nonstationary concentration spectrum and nonstationary sampling error filter) and the evaluation of the sampling network should be done in real time by taking advantage of the information gained from the previously collected measurements.

APPENDIX: FOURIER TRANSFORM OF DISCRETE SAMPLING FILTER $\hat{p}(l)$

The linear filter corresponding to the discrete averaging process in the one-dimensional example is given as

$$\hat{p}(l) = \frac{\Delta l}{L} \sum_{n=0}^{N-1} \delta[l - n\Delta l] \qquad x - L/2 \le l \le x + L/2 \tag{30}$$

$$\hat{p}(l) = 0 \qquad \text{otherwise}$$

The Fourier transform of $\hat{p}(l)$ can be written as

$$\hat{P}(k) = \mathcal{F}(\hat{p}(l)) = \int_{-\infty}^{\infty} \frac{1}{N} \sum_{n=0}^{N-1} \delta(l - n\Delta l) e^{-ikl}\, dl \tag{31}$$

where k is the wave number, $\delta(\ )$ is the delta function, and $\mathcal{F}$ denotes Fourier transform. Using the shifting property of the delta function the above can be written as

$$\hat{P}(k) = \frac{1}{N} \sum_{n=0}^{N-1} e^{-ik\Delta l}$$

$$= \frac{1}{N} [1 + e^{-ik\Delta l} + e^{-ik2\Delta l} + \cdots + e^{-ik(N-1)\Delta l}] \tag{32}$$

which represents a power transfer function described as a summation of negative exponentials. This expression can be written as [*Blackman and Tukey*, 1959, p. 131]

$$\hat{P}(k) = \frac{B(kN\Delta l/2)}{B(k\Delta l/2)} = \frac{1}{N} \frac{\sin(kN\Delta l/2)}{\sin(k\Delta l/2)} \tag{33}$$

which completes the evaluation of the Fourier transform of $\hat{p}(l)$.

Acknowledgments. R.A. was supported by a grant from the Legislative Commission on Minnesota Resources and E.F.-G. by grant BSC-8957469 from the National Science Foundation. Computer time on a Cray-2 supercomputer was provided by the Minnesota Supercomputer Institute. We thank Dennis McLaughlin for reviewing this manuscript and providing valuable input and Hugo Loaiciga for his comments and for handling our paper as Associate Editor.

REFERENCES

Andricevic, R., Cost-effective network design for groundwater flow monitoring, *Stochastic Hydrol. Hydraul.*, *4*(1), 27–41, 1990*a*.

Andricevic, R., A real-time approach to management and monitoring of groundwater hydraulics, *Water Resour. Res.*, *26*, 2747–2755, 1990*b*.

ASCE Task Committee on Geostatistical Techniques in Geohydrology, Review of geostatistics in geohydrology, I, Basic concepts, *J. Hydraul. Eng.*, *116*(5), 612–632, 1990*a*.

ASCE Task Committee on Geostatistical Techniques in Geohydrology, Review of geostatistics in geohydrology, II, Applications, *J. Hydraul. Eng.*, *116*(5), 633–659, 1990*b*.

Bakr, A. A., L. W. Gelhar, A. L. Gutjahr, and J. R. McMillan, Stochastic analysis of spatial variability in subsurface flows, 1, A comparison of one- and three-dimensional flows, *Water Resour. Res.*, *14*, 263–271, 1978.

Blackman, R. B., and J. W. Tukey, *The Measurement of Power Spectra*, Dover, New York, 1959.

Bras, R. L., and I. Rodriguez-Iturbe, *Random Functions in Hydrology*, Addison-Wesley, Reading, Mass., 1985.

Carrera, J., E. Usunoff, and F. Szidarovszky, A method for optimal observation network design for groundwater management, *J. Hydrol.*, 73, 147–163, 1984.

Gelhar, L. W., and C. W. Axness, Three-dimensional analysis of macrodispersion in aquifers, *Water Resour. Res.*, *19*, 161–180, 1983.

Graham, W., and D. McLaughlin, Stochastic analysis of nonstationary subsurface solute transport, 1, Unconditional moments, *Water Resour. Res.*, *25*, 215–232, 1989*a*.

Graham, W., and D. McLaughlin, Stochastic analysis of nonstationary subsurface solute transport, 2, Conditional moments, *Water Resour. Res.*, *25*, 2331–2357, 1989*b*.

Hsu, N.-S., and W. W.-G. Yeh, Optimum experimental design for parameter identification in groundwater hydrology, *Water Resour. Res.*, *25*, 1025–1040, 1989.

Hsueh, Y. W., and R. Rajagopal, Modeling groundwater quality sampling decisions, *Ground Water Monit. Rev.*, *8*, 121–134, 1988.

Kumar, P., and E. Foufoula-Georgiou, A stochastic simulation model for space-time description of rainfall, *Tech. Rep. M-219*, 124 pp., St. Anthony Falls Hydraul. Lab., Univ. of Minn., Minneapolis, 1989.

Li, S. G., and D. McLaughlin, A nonstationary spectral method for solving stochastic groundwater problems: Unconditional analysis, *Water Resour. Res.*, *27*, 1589–1605, 1991.

Loaiciga, H., An optimization approach for groundwater quality monitoring network design, *Water Resour. Res.*, *25*, 1771–1782, 1989.

Massmann, J., and R. A. Freeze, Groundwater contamination from waste management sites: The interaction between risk-based engineering design and regulatory policy, *Water Resour. Res.*, *23*, 351–367, 1987.

McLaughlin, D., and W. Graham, Design of cost-effective programs for monitoring groundwater contamination, *IAHS Publ.*, *158*, 1986.

Meyer, P. D., and E. D. Brill, A method for locating wells in a groundwater monitoring network under uncertainty, *Water Resour. Res.*, *24*, 1277–1282, 1988.

Morrison, D., and R. Andricevic, Heterogeneity in the hydraulic conductivity and its impact on the solute transport, *Tech. Rep. 314*, 187 pp., St. Anthony Falls Hydraul. Lab., Univ. of Minn., Minneapolis, Feb. 1991.

Moss, M. E., Space, time and third dimension (model error), *Water Resour. Res.*, *15*, 1797–1800, 1979.

North, G. R., and S. Nakamoto, Formalism for comparing rain estimation designs, *J. Atmos. Oceanic Technol.*, *6*(6), 985–992, 1989.

Olea, R. A., Sampling design optimization for spatial functions, *Math. Geol.*, *16*(4), 365–391, 1984.

Perlmutter, N. M., and M. Lieber, Disposal of plating wastes and sewage contaminants in the groundwater and surface water, South Farmingdale-Massapequid area, Nassau County, New York, *U.S. Geol. Surv. Water Supply Pap.*, *1879-G*, 1970.

Rodriguez-Iturbe, I., Scale of fluctuation of rainfall models, *Water Resour. Res.*, *22*(9), 15S–37S, 1986.

Rouhani, S., Variance reduction analysis, *Water Resour. Res.*, *21*, 837–846, 1985.

Rubin, Y., Stochastic modeling of macrodispersion in heterogeneous porous media, *Water Resour. Res.*, *26*, 133–143, 1990.

van Geer, F. C., Applications of Kalman filtering in the analysis and design of groundwater monitoring network, *Tech. Rep. PN 87-05*, TNO-DGV Inst. of Appl. Geosci., Delft, Netherlands, 1987.

Vanmarcke, E., *Random Fields*, MIT Press, Cambridge, Mass., 1983.

Vomvoris, E. G., and L. W. Gelhar, Stochastic analysis of the concentration variability in a three-dimensional heterogeneous aquifer, *Water Resour. Res.*, *26*, 2591–2602, 1990.

R. Andricevic and E. Foufoula-Georgiou, St. Anthony Falls Hydraulic Laboratory, Civil and Mineral Engineering Department, University of Minnesota, Minneapolis, MN 55414.

(Received February 25, 1991;
revised May 16, 1991;
accepted May 21, 1991.)